

Estimates of Meridional Heat Transport in The South Atlantic Ocean

Silvia L. Garzoli and Molly O. Baringer

NOAA Atlantic Oceanographic and Meteorological Laboratory,
Miami, FL 33149. USA.

silvia.garzoli@noaa.gov

molly.baringer@noaa.gov

Submitted to Journal of Marine Research

July 2005

Abstract

Upper ocean temperature data collected nominally along 35°S in the South Atlantic are analyzed to obtain estimates of the meridional heat transport. Temperature data is obtained from high-density XBT profiles with horizontal spacing of 10-50 km to depths of about 800 meters on transects from Cape Town, South Africa to Buenos Aires, Argentina that occur approximately four times each year thanks to voluntary observing ships. Salinities are estimated for each XBT temperature observation, from statistical relationships between temperature, latitude, longitude and salinity computed along depth surfaces using data obtained from Argo profiles and CTD casts. Full depth profiles are obtained by extending the profiles to the bottom of the ocean using deep climatological data. The meridional transport is then determined by using the standard geostrophic method, applying NCEP-derived Ekman transports and assuring mass is conserved. The heat transport values obtained with this methodology using data collected during the World Ocean Circulation Experiment (WOCE) along the A10 hydrographic transect and the output from a numerical model compare favorably with other estimates and direct model integrations. Ten XBT sections collected between July 2002 and May 2005 are analyzed. The mean meridional heat transport obtained is 0.73 with a standard deviation of 0.15 PW (1PW = 10^{15} Watts) when using $\sigma_0=27.4$ kg m^{-3} as the reference level and 0.67 with a standard deviation of 0.17 PW for a reference level at $\sigma_2=37.09$ kg m^{-3} . It is shown that the use of smooth climatology data for the deep ocean ($Z > 850$ m) appears to introduce a positive bias of 0.2 PW. This suggests the estimated XBT-derived heat transports may be artificially high due to the smoothed subsurface climatology used and hence an additional uncertainty of 0.2 PW cannot be ruled out. In any regard, these values are in agreement with the ones provided from numerical models, and with the mean of previous calculations that ranged from -0.2 to

1.0 PW. The values obtained do not show a clear seasonal cycle. However, ten realizations are not enough to resolve a seasonal cycle in the presence of large interannual variability.

I. Introduction

Meridional heat flux in the ocean is a key element of the climate system because of the role that the ocean plays in determining the Earth's climate through its interaction with the atmosphere. In order to understand and predict climate variability, it is crucial to understand the mechanisms and the pathways of mass and heat transport in the global ocean. Despite its small size, the Atlantic Ocean is responsible for over half of the northward heat transport carried by the global ocean. This ocean meridional heat flux is due in part to a worldwide vigorous circulation that connects all the basins, the meridional thermohaline circulation. In the South Atlantic, this meridional overturning circulation is composed of northward transports of warm surface and intermediate layer waters in the upper 1200m, southward transport of North Atlantic Deep Water, and northward flowing Antarctic Bottom Water. As such, the South Atlantic Ocean is a necessary conduit for the warm upper layer water that flows northwards across the equator, compensating for the colder southward flowing North Atlantic Deep Water. The South Atlantic Ocean connects the three major ocean basins: the Pacific Ocean, the Atlantic Ocean and the Indian Ocean. The meridional gaps between the continents of the Southern Hemisphere and Antarctica allow for a free exchange of water between the basins. Presently, the mean pathways of the circulation have been only vaguely quantified. The main debate is still focused on the relative importance of the interocean exchange between the Indian and the Atlantic Oceans. Gordon *et al.* (1992) concluded

that the major proportion of the export of deep water from the North Atlantic is balanced by northward flow of lower thermocline and intermediate water through the South Atlantic Ocean which is a local mixture of Indian and Pacific waters entering the basin as Agulhas Current leakage and through the Drake Passage, respectively.

Based on the data collected during the World Ocean Circulation Experiment (WOCE), Stramma and England (1999) examined the water mass distribution and circulation patterns at different depths of the South Atlantic. They simplified the circulation into a layered scheme that can be summarized as follows (Figure 1): the Deep Western Boundary Current (DWBC) transports North Atlantic Deep Water (NADW) from the northern hemisphere into the South Atlantic at depths near 2000 m (Figure 1). The Antarctic Intermediate Water (AAIW) originates in the South Atlantic from a near surface region of the Circumpolar Current, especially in the Northern Drake Passage and the Malvinas Current Loop. AAIW from the Indian Ocean joins the South Atlantic AAIW via the Agulhas leakage that includes northward flow within the depth of the intermediate water layer (500 to 1200m). South Atlantic Central Water (SACW) carried in the Brazil Current mixes with Indian Ocean Central Water brought into the Atlantic Ocean by the Agulhas Current intrusions. It flows in the upper layers between 100 and 500 m, following a more meridional pathway than the purely zonal flowing AAIW as they transit from the eastern to western boundaries. The circulation shows a southward shift with depth within the subtropical gyre. In the same study Stramma and England (1999) used a coarse resolution global ocean GCM and a global eddy-permitting model to assess the ability of the models to capture the observed circulation. Both models resolved the

southward shift of the gyre but neither model was able to reproduce the zonal current system in the south Atlantic.

Donners and Drijfhout, (2004) analyzed the product of a global ocean general circulation model (OCCAM) to investigate the interocean exchange of thermocline and intermediate waters in the South Atlantic using a Lagrangian path-following technique. Results of the analysis suggest that most of the South Atlantic upper layer limb of the MOC is derived from Agulhas leakage. More than 90% of the flow towards the North Atlantic originates from the Indian Ocean via leakage from the Agulhas Current system. Agulhas leakage into the South Atlantic occurs from the surface to depths as great as 2000 m. This relatively warm water (higher than 10°C on average) leads to relatively large meridional heat fluxes in the band 30° to 35°S . From the same product, de Ruijter et al. (2004) calculated the time variable heat flux at 30°S and found the mean annual value for the heat transport is 0.58 PW and a marked annual cycle with values ranging from 0.5 to 1.1 PW.

Numerous studies have been conducted to calculate the heat transport in the global ocean using different methods. These include direct observations (e.g., Macdonald *et al.*, 2001; Talley, 2003), inverse models (e.g. Ganachaud and Wunsch, 2003, Rinotul, 1991, Fu, 1981) and numerical models (e.g. Matano and Philander, 1993; Saunders and Thompson, 1993; Saunders and King, 1995). Within the subtropical region, in the 30° to 35°S band, the northward heat flux estimates range from negative values (-0.23 PW, de las Heras and Schlitzer, 1999) to more than 1 PW (0.94 PW, direct method, Saunderson and King 1995; 0.88 PW, Inverse model Fu, 1981).

To some extent the heat transport differences between the models is a consequence of their ability to reproduce the pathways of the intermediate water and to represent the variability of the boundary currents. In the observations, differences between estimates may be a consequence of the different methods to calculate the heat transport. However, large heat transport variability may be a real feature of the South Atlantic circulation due in part to the large variability of the boundary currents. Both margins are characterized as highly energetic and variable regions.

In 2002 as part of the NOAA Global Ocean Observing System, a new expendable bathythermograph (XBT) high-density line was started in the South Atlantic between Cape Town, South Africa and Buenos Aires, Argentina. The line is referred to as AX18. Before 2004, the line was sampled twice a year. Since 2004 four occupations per year are conducted. The line was conceived to monitor the upper layer mass budget in the South Atlantic and to estimate the variability of the upper limb of the MOC transport. Up to date 10 transects are available (Figure 2). In this paper, estimates of the meridional mass and heat transport obtained from the data collected along AX18 are presented.

II. The current systems at the boundaries

The western boundary

The upper ocean circulation in the Southwestern Atlantic is characterized by the encounter between the warm and saltier southward-flowing Brazil Current and the cold and fresh northward-flowing Malvinas Current. This encounter takes place at approximately 38°S and creates a strong thermohaline front with temperature gradients as high as 1° C/100 m that has been given the name of the Confluence Front (Gordon and Greengrove, 1986) and thereafter, the Confluence. The Brazil Current is the western boundary current of the subtropical South Atlantic Ocean, one of the weakest in the world's oceans. Its poleward (southward) transport varies with latitude reaching values no larger than 30 Sv, most of it confined to the upper 1000 m (Gordon and Greengrove, 1986; Garzoli, 1993). Being a weak current, the intensity of the Brazil Current transport can be influenced by the local wind stress (Gordon and Greengrove, 1986; Olson *et al.*, 1988). In the southwest region of the South Atlantic basin, the Malvinas Current, a branch of the Circumpolar Current, is the main conduit of Pacific water into the subtropical Atlantic. This current flows north along the eastern edge of the continental shelf of Argentina to latitudes as far north as 33°S (Garzoli, 1993; Piola and Gordon, 1989). The Malvinas Current is mostly uniform with depth and hence estimates of the volume transport traditionally obtained from hydrographic data using a level no motion at the bottom of the AAIW vary between 10 and 15 Sv (Gordon and Greengrove, 1986; Garzoli, 1993). However, mass conservation in the region points toward the presence of significant bottom velocities along the continental slope near the Brazil Malvinas Confluence. Peterson (1992) used an inverse calculation and obtained top to bottom values for the Malvinas Current transport ranging from 70 to 80 Sv between 42° and 46°S. These values are consistent with those obtained from some models (Cox, 1975; Semtner and Chervin, 1992, Webb et al., 1991). Current meter

measurements of the Malvinas Current gathered between December 1993 and June 1995 near its merger with the Brazil Current (between 40 and 41°S) observed a mean transport of 30 Sv with a variability of about 12 Sv root mean squared (Vivier et al., 2001).

The Brazil/Malvinas confluence is one of the most energetic regions in the world ocean (Chelton et al., 1988). A marked variability in the location of the Confluence front by up to 900 km along the coast has been observed both from surface observations (Olson *et al.*, 1988) and subsurface observations (Garzoli and Bianchi, 1987; Garzoli and Garraffo, 1989). During the austral summer (January, February, March), the Brazil Current reaches its southernmost extension when the Malvinas Current retreats (Garzoli *et al.*, 1992). An opposite situation is observed during the austral winter (June, July, August) when Malvinas waters reach their northernmost latitudes. Significant interannual variability has also been observed (Olson *et al.*, 1988; Garzoli, 1993). Garzoli and Garraffo (1989) suggested that remote influences on this variability could be two fold: an intensification of the winds in the Southern Ocean and variability in the South Equatorial Current (SEC). Peterson (1988) observed a direct relationship between the magnitude of the winds in the Southern Ocean and the transport of the Antarctic Circumpolar Current (ACC), which Garzoli and Garraffo (1989) linked to the strength of the Malvinas Current. After the Confluence, both currents turn eastward and flow offshore in a series of large-scale meanders (Gordon and Greengrove, 1986; Reid, 1989).

The continental shelf of Argentina is the widest of the world ocean (Mazio et al., 2004). Its width varies from 160 km at approximately 37°S to 740 km at 52°S with a length of

2400 km. The area is characterized by a smooth slope and smooth relief (Parker et al., 1997). The average depth is 50 m, gently sloping to approximately 250 m just before reaching the continental slope. Palma et al., (2004) conducted a careful analysis of the currents along the Argentine continental shelf. They analyzed the modeled oceanic circulation patterns over the shelf forced by nine different wind climatologies. Results indicate that at 35°S there is a weak northward transport that varies between 0.0 and 0.2 Sv, depending on the wind climatology.

The eastern boundary

The South Atlantic thermocline and subantarctic inflow is derived from the eastward flowing South Atlantic Current (Stramma and Peterson, 1990) part of which turns northward into the Benguela Current. The Benguela Current is the broad northward flow adjacent to southwestern Africa that forms the eastern limb of the South Atlantic subtropical gyre and the origin of upper layer water that flows northward across the equator into the North Atlantic. The Indian Ocean water is injected into the Benguela Current through Agulhas eddy shedding and the Agulhas Retroflexion filament processes (Lutjeharms and Van Ballegoyen, 1988; Shannon *et al.*, 1989). At 30°S, the entire Benguela Current is confined between the African coast and the Walvis Ridge near the Greenwich Meridian. Observations reveal that at 30°S the Benguela Current transport consists of a nearly steady flow confined between the southern African coast and approximately 4°E (amounting to 10 Sv in the mean) and a more variable flow (3 Sv in the mean) between 4°E and the Walvis Ridge (Garzoli and Gordon, 1996). It has also been observed that a minimum of four to six rings originating from the Agulhas Retroflexion enter the Cape Basin each year (Duncombe Rae *et al.*, 1996) and that the

eddy field is responsible for the transport of 0.007 PW and 2.6-3.8 Sv between the two basins. Goñi *et al.*, (1997) use the BEST data set and TOPEX/POSEIDON-derived maps of upper layer thickness to estimate that five, four, and six rings were shed from the Agulhas Current during 1993, 1994, and 1995, respectively, with an average of 1 Sv contributed by each ring to the volume transport of the Benguela Current into the South Atlantic Ocean. After crossing 30°S, the Benguela Current turns westward forming what is called the Benguela Extension. The boundaries of the Benguela Current extension are defined through the analysis of Rafos float trajectories deployed as part of the Benguela Current Experiment (Richardson and Garzoli, 2003). Results indicate that at 750 m the Benguela extension is bounded to the south by 35°S and to the North by an eastward current located between 18°S and 21°S. The westward transport of the Benguela Extension is estimated to be 15 Sv. Roughly 1.5 Sv of this is transported by the approximately 3 Agulhas rings that cross the mid-Atlantic ridge each year (Richardson and Garzoli, 2003). Geostrophic shear in the Benguela Current and its extension is very small suggesting that this current is only weakly baroclinic (1-2 cm/sec over 1000m). The total westward transport in the Benguela Current Extension above 1000 m and between 18°S-33°S is estimated to be 29 Sv.

Along the inner shelf of South Africa, Bang (1974) using direct current measurements, found a strong equatorward jet southwest of Cape Town. This jet is confined to the midwater and surface layers and to a strip of 5 nautical miles wide. According to Shannon and Nelson (1996), the estimated mean transport of this current is 1 Sv. Compensating for the vertical displacement of water on the inner shelf and its movement northward is a narrow strip of southward flow found at the base of the shelf

(Nelson, 1989). This poleward flow is part of a more extensive poleward motion stretching from the coast across the shelf and out into the Cape Basin as far as 17° 35'E (Shannon and Nelson, 1996; Nelson, 1991). South of 33°S, the principle region of interest for this paper, the flow is not seasonally dependent.

III. Methodology

Direct estimates of meridional volume (V) mass (M) and heat (H) transport require the knowledge of the temperature (T), salinity (S) and meridional velocity (v) fields:

$$V = \int v dx dz \quad [S_v = 10^6 m^3 / s]$$

$$M = \int \rho v dx dz \quad [Kg / s]$$

$$H = \int \rho c_p T v dx dz \quad [PW = 10^{15} Watts]$$

where ρ is the density of the water and c_p the specific heat capacity.

The total meridional velocity (v) can be decomposed into 3 components:

$$v = v_b + v_g + v_{ag}$$

v_b is the barotropic component, v_g is the geostrophic (baroclinic) component that can be estimated from the hydrographic field, and v_{ag} is the ageostrophic component that is often assumed to be due to wind forcing and given by the Ekman transport. Meridional Ekman transports are computed as the Ekman mass M_y and Ekman heat H_y transport:

$$M_y = - \frac{\tau_x}{f} D$$

$$H_y = M_y c_p T$$

where τ_x is the zonal component of the wind stress, f the Coriolis parameter and T is the mean temperature of the Ekman layer.

The methodology used to obtain the baroclinic component of the heat transport from the expendable bathythermograph (XBT) data collected along AX18 is as follows: the XBT data are collected using an automated launcher with a Sippican Mk 12 circuit board and GPS receiver that stores 6-8 XBTs that are deployed at specified time or space intervals. XBT data from Sippican T-7 XBTs consist of temperature time series collected every 0.1 seconds that typically extend to depths of about 850 meters. The temperature time series is converted into a depth profile using the updated fall-rate equation of Hanawa et al. (1995). In this paper, salinity (S) is estimated for each XBT profile by using two-dimensional fields of S (T,p) relationships at different locations created by Thacker following the methodology described by Thacker et al., (2004) for the South Atlantic using ARGO profilers and CTD data available in the region. Where insufficient CTD and ARGO data are available, the World Ocean Atlas 2001 (WOA01) gridded annual climatology (Stephens et al., 2002) is used to estimate S(T). In order to obtain the heat transport across the section, the total mass transport must be zero (i.e. mass must be conserved). The XBT probes samples the ocean only up to about 850m, hence the data are extended to the bottom using the WOA01 gridded climatology

bathymetry by interpolating the data to the location of each XBT to generate an annual mean climatology for the deep ocean. The bottom is determined to be the depth at the location of the XBT from the Smith and Sandwell 2 minute data base bathymetry (Smith and Sandwell, 1997).

Geostrophic velocities are determined using the dynamic method where a level of no motion was chosen at a depth just below the northward flowing AAIW at $\sigma_0=27.4 \text{ kg m}^{-3}$ (σ_0 defined as potential density relative to the surface) and $\sigma_2 = 37.09 \text{ kg m}^{-3}$ (σ_2 defined as potential density relative to 2000 dbar) to compare with previous results. Ekman transports are determined using NCEP climatological monthly mean reanalysis winds by interpolating the NCEP values to the location of the XBT observation. Transports are computed in layers and summed for the entire water column. A simple constant reference velocity for each section is applied at the reference level so that the net mass transport across the section is zero. Typically, values of this velocity are in the range of 10^{-4} to 10^{-6} m s^{-1} . As explained later, additional corrections to the net transports are made when needed to account for barotropic motions and for XBT sections that failed to terminate at the 200 m isobath or shallower on each side of the Atlantic.

III. Sensitivity of the methodology and errors.

Possible uncertainty in the findings can result from the assumptions applied including: the simple mass balance geostrophic method, the uncertainty in salinity assigned to each temperature observation, the representativeness of Levitus data below 800 m, and the variable latitudes that each XBT section crosses the Atlantic. Sensitivity to these factors and others such as the specific wind climatology used and its inherent

uncertainty are discussed in this section. In order to test the validity of the methodology, data from the WOCE A10 line (Siedler et al., 1996) is used in the simple geostrophic method to compare heat transports estimates. A10 data can be systematically reduced to temperature data in the upper 850 m to simulate XBT data and the resultant heat transport will indicate what sort of errors can be found from using real XBT transects. The POCM model heat transport is also analyzed to examine the possible errors from uncertainty in barotropic motions.

A10 Heat Transport: Simulating XBTs

A10 is nominally along 30°S, collected during January 1993 and provides temperature and salinity as a function of depth for the whole water column across the entire South Atlantic Ocean. Ganachaud and Wunsch (2003) recently analyzed the A10 data using the geostrophic method with corrections applied based on an inverse model to estimate the meridional heat transport across 30°S (see Table 1). Ganachaud and Wunsch (2003) uses a deep reference level approximately between Antarctic Bottom Water (AABW) and North Atlantic Deep Water (NADW) along a neutral density of 28.11 (equivalent to $\Theta \sim 1.9^\circ\text{C}$ or $\sigma_2 = 37.07 \text{ kg m}^{-3}$) and constrain the solution to have 4 ± 0.4 Sv of AABW flowing north in the western basin and 0 ± 1 Sv from below approximately 4000m to the east of 7°W. Figure 3 shows the vertical distribution of temperature and the density levels from A10 data. To calculate the Ekman transport Ganachaud and Wunsch (2003) use annual mean NCEP climatological winds. In a recent paper by McDonagh and King (2005) using a box inverse model, recalculated the heat flux across A10 and obtained the value of 0.22 ± 0.08 PW, a number considered to be in agreement with previous results.

The methodology described in the previous section is applied to the values of $T(z)$ and $S(z)$ collected along A10 to obtain direct estimates of heat transport (Table 1, line 2). In particular, mass transport is computed from the surface to bottom and adjusted to be zero across the section. Volume and heat transport are computed. Total volume and heat transport are calculated by adding Ekman transport. In all of the A10 cases described in this section, the Ekman transport is obtained using NCEP annual climatological winds to match Ganachaud and Wunsch (2003) results. The results listed in Table I indicate that the basic methodology applied produces an insignificant difference to the meridional heat transport: the inverse method used by Ganachaud yields a value of 0.4 PW ($1\text{PW} = 10^{15}$ Watts) (Table I, Line 1), while the direct method given herein gives a similar value: 0.41 PW (Table I, Line 2).

XBTs, however, contain no salinity information. This deficiency can be simulated with A10 data, by considering the $T(z)$ values from A10, and prescribing the salinity above 850 m from the functions of temperature, depth and geographic location provided by Thacker (2004). Heat transport using the above methodology is then computed as 0.45 PW (results in Table 1, line 3). Salinities estimated in this way change the computed value in heat transport only slightly.

XBTs only sample the upper 850 m of the water column and hence some estimate of the subsurface values must be made. A10 data is used such that $T(z)$ above 850 m is obtained directly from A10. Salinity above 850 m is inferred using the relations provided by Thacker (personal communication). Below 850 m the WOA01 annual mean $T(z)$ and

S(z) field is used. Heat transport is estimated as 0.66 PW following the previously described methodology (results in Table 1, line 4). By far the largest difference is found when the deep values of T and S collected along A10 are replaced by the WOA01 climatology below 850 m. In this case there is a positive difference of more than +0.2 PW.

Using full water column CTD data, the depth at any location is typically known to within about 10 m. With XBTs the depth must be determined from the Smith and Sandwell database. Using the A10 data as if it were an XBT and the depth was determined from Smith and Sandwell instead of the maximum depth provided by the CTD cast, the heat transport is estimated to be 0.69 PW (results in Table 1, line 5). This value can be most directly compared to using the actual CTD depth (Table 1, line 4) and hence shows that there is very little error induced by not knowing the exact water depth (an additional change of 0.03 PW).

For XBT data, a shallow reference level just below AAIW is used, which is particularly appropriate for the Benguela Current region, while Ganachaud and Wunsch, (2003) use a deep reference level. For comparison, all the above A10 cases have been computed using the deeper reference level (Table 1, second column). Heat transports estimates computed using a shallower reference level at a layer just below the northward flowing AAIW yield in this case larger values than the ones estimated with a reference level close to the bottom.

POCM Heat Transport:

Additional uncertainty in the results may be due to the simplicity of the geostrophic method used that applies to both Ganachaud and Wunsch (2003) and our results. In particular, the role of the barotropic field and deep boundary currents. In what follows the POCM numerical model (Tokmakian and Challenor, 1999) is examined to compare results estimated from the total velocity field to those obtained from geostrophic velocities.

1. From the model velocity field, the volume and heat transports are computed for 30°S and 35°S. Some of the results for 35°S are shown in Figure 4. The time series of heat transport for the model years 1986 to 1998 indicate a strong interannual variability with values between 0.2 and 1.1 PW. The mean value of the series at 30°S is 0.55 PW and 0.57 PW at 35°S with a standard deviation of 0.16 PW and 0.19 respectively. The model mean annual cycle exhibits a maximum in the month of July and a minimum in the month of February (Figure 4). Not shown is the vertical distribution of the geostrophic and heat transport that indicates that all of the northward flow is contained above the upper kilometer of the ocean above the AAIW.
2. The geostrophic transports are calculated using the T and S fields from the model fields by using the geostrophic method with a reference level at $\sigma_0 = 27.4$ kg m⁻³. Transports are adjusted as described above to balance mass. Results are 0.85 PW at 30°S and 0.80 PW at 35°S, that is to say, 0.30 PW larger than when computed directly from the velocity field. These results indicate that there is a component of the flow that is not being taken into account using a simple uniform reference velocity on a single surface. Through further inspection of the

model fields, a barotropic component was observed located west of 45°W with southward bottom velocities having a mean of 0.06 m/sec. This barotropic flow is the result of the Brazil Current and the deep Atlantic North water flowing in the same direction. Current meter measurements at 35°S confirm bottom velocities of the order of 0.04 to 0.06 m/sec, (Flood and Shore, 1988). That is to say, in order to obtain a realistic value for the heat transport from the data collected along AX18, it is necessary to correct for the barotropic component of the field at the western boundary. When the heat transport values obtained from the model T and S are corrected for the barotropic component of the flow (by adding a bottom velocity of -0.031 m sec⁻¹ at 30°S and -0.025 m/sec at 35°S for all station pairs west of 45°W, which are the mean values from the model), results for the heat transport are 0.60 PW at 30°S and 0.50 PW at 35°S, similar to the ones obtained by using the model velocity field.

Finally, the uncertainty resulting from using different wind products to compute the Ekman fluxes are estimated. The total heat flux is obtained as the sum of the geostrophic plus Ekman components. Therefore, the wind products used and their variability in the region are another source of uncertainty in obtaining heat fluxes estimates. The Ekman flux was obtained from computing a monthly climatology from monthly NCEP reanalysis winds provided by NOAA-CIRS Climate Diagnostic Center, via their web site at <http://www.cdc.noaa.gov>. Results are shown in Figure 5 as a function of month and latitude. Averaged mixed layer properties used to calculate the heat transport are obtained from the WOA01 climatology; results are very similar when using XBT derived values. The maximum positive value of the Ekman heat flux, 0.35

PW, is observed during July at 38°S. The zero contour line migrates meridionally between 28° and 34°S following an annual and semiannual signal. In addition to natural variability of the fluxes, there is a possible ambiguity in interpreting the time variability of the XBT-derived heat transport estimates due to the fact that each vessel deploying XBTs may follow different routes across the ocean basin, hence sampling different latitudes within a strongly varying wind field. This uncertainty could be as much as 0.5 PW (e.g. if comparisons were made between heat transport estimates in March at 30°S and heat transport estimates in June at 37°S) and hence by far the largest variability is natural, reflecting space and time differences. Ekman fluxes were also calculated from Hellerman and Rosenstein (1983) winds and from satellite winds (not shown). Results indicated that due to the use of different wind products the values obtained for the heat transport across 35°S varied by less than ± 0.1 PW, indicating all products show similar variability.

Based on the analysis of the model, geostrophic transports obtained from the data collected along the AX18 transects are corrected by using a bottom velocity in the region of the Brazil Malvinas region given by Peterson (1992) of $v = -0.04$ m/sec. The extent of the area in which the correction is applied, is determined by the resultant value of the deep current (in the mean, 10 to 15 Sv). After the bottom velocity correction is applied, transports are evaluated again to adjust for conservation of mass across the entire basin. The sensitivity of the results to the selected value of v was analyzed. Results indicate that by increasing v by as much as $\pm 20\%$, the results on the heat transport varied by only ± 0.02 PW.

In summary, different wind products introduces an uncertainty of ± 0.10 PW in heat transport estimates. The uncertainty about the depth of the bottom of the ocean introduces an error of ± 0.02 PW. At the western boundary, the correction for bottom velocity leads to an additional uncertainty of ± 0.02 PW. If the uncertainty due to the flow over the Argentine continental shelf is added (± 0.01 PW) and a similar value is assumed at the eastern boundary (± 0.01 PW) the total uncertainty is about ± 0.16 . Recall that the difference between using the WOA01 data below 850 meters along A10 and the full A10 section was 0.2 PW. The use of a smooth climatology for the lower layers introduced an additional uncertainty of 0.20 PW to the heat transport estimates which we assume is a bias due to the smoothed nature of the deep fields “smearing out” density gradients that should carry the lower limb of the MOC through geostrophic shear. This assumption is anecdotal and based solely on one section and hence may not be constant in time or space, but based on this we believe our estimates to be as much as 0.2 PW high, as well as containing an overall uncertainty of 0.16 PW.

IV. Heat transport from the AX18 data

In this section the analysis of the heat transport across AX18 is presented. Estimates are obtained using a reference level of $\sigma_0 = 27.4 \text{ kg m}^{-3}$ and $\sigma_2 = 37.09 \text{ kg m}^{-3}$. Occasionally due to weather, equipment malfunctions etc., XBT sections have not completely crossed the entire Atlantic basin (e.g. to approximately the 200 m isobath). Table II lists the western and easternmost stations and the beginning/ending ocean depths for all the sections taken to date. In particular, sections in July 2002, Nov 2002 and July 2004 were commenced late or terminated early. These sections have failed to sample all the water and hence strict mass conservation is not possible. Also there is

always a small portion of the flow on the continental shelf that is not captured by the measurements.

For the western boundary, according to Palma *et al.* (2004) the transports in the shelf at latitudes close to 35°S range from 0.0 to 0.2 Sv. After balancing the section for conservation of mass, a northward or southward flow of 0.2 Sv introduced a change in the heat transport of less than ± 0.01 PW, a value that is below the other uncertainties. The only case in which a correction due to the section missing a portion of the western boundary currents was necessary was for November 2002. Corrections applied to this section are outlined in detail below.

For the eastern boundary, the net contribution to the heat transport from the coast up to 17.5°E is negligible due to the compensating northward and southward coastal currents discussed previously (Nelson, 1991). An extremely conservative estimate of the mean temperature differences between these currents (5°C), leads to an estimated heat transport of less than 0.01 PW. The only cases in which a correction is needed is therefore for the sections collected during July 2002 and 2004 when the first station was obtained at 16.66°E and 13.83°E respectively. Corrections to the July 2004 section are described in detail below. The correction for the July 2002 section (not shown) follows the same procedure.

In what follows are detailed descriptions of three example sections: one section with no correction and the two sections November 2002 and July 2004 with transport corrections.

March 2004

This cruise was conducted along 35°S. The cruise track is shown in Figure 6 plotted over the wind field (top panel) and the SST field (lower panel). The wind field was obtained from the NCEP reanalysis and is an average over the duration of the cruise (days 76 to 107, 2004). According to previous observations (Garzoli and Garraffo, 1989; Goni and Wainer 2001), at this time of the year the Malvinas Current should have been retracted from its northernmost extension and should no longer be present in the area. The SST satellite image (Figure 6, lower panel) shows that this is indeed the case. The Brazil Current is at its southernmost extension, south of 37.5°S. The easternmost XBT station hit the bottom at 272 m and the westernmost XBT reached 129 m depth (i.e. over the shelf). Therefore, the section completely crossed the ocean basin and hence no correction is required to estimate missing transport. The uncertainty is the one estimated before and the estimated heat transport is 0.78 ± 0.16 PW.

November 2002

This line was conducted along approximately 35°S latitude. According to the historical record, the Malvinas Current should be receding from its northernmost extension during this time of year. The SST satellite image (Figure 7) shows that during November 2002 there is a strong SST front near 36°S, i.e. its location is slightly to the north of its expected mean position of the Malvinas Current for that month. Most of this SST front is on the shelf and contains a mixture of water from the relatively cold and fresh

southern shelf water, the Rio de la Plata outflow (La Plata River) and the southward flowing Brazil Current.

The estimated heat transport across the section is 0.47 ± 0.17 PW. The westernmost XBT station was collected in 832 m of water (i.e. on the continental slope). Therefore, it failed to sample a portion of the shelf water and its return flow along the continental shelf (that should be compensating each other) and a portion of the Brazil Current along the continental shelf slope typically positioned between the 200 to 830 m isobaths. The SST map (lower left panel, Fig. 6) indicates a Brazil Current ring ready to detach from the main BC flow centered at approximately 36°S 49°W . This is confirmed by the sea surface height derived from altimeter data (Goni, personal communication, Figure 8). The missing transport can be estimated from the dynamic height field shown in Figure 8. Assuming that the ring is symmetric, the result is a small missing flow of 0.18 Sv. This small transport correction leads to a change in the heat transport of -0.01 PW. This correction is estimated as:

$$\Delta\text{HT} = \Delta V (T_m - T) c_p \rho_0$$

where ΔV is the missing mass volume transport, T_m is the mean temperature of the section, T is the temperature of the missing flow, c_p is the specific heat and ρ_0 , the density of water. With this correction, the total heat transport is 0.46 PW. If the correction for missing flow (0.18 Sv) has an error of 100% (± 0.18 Sv), this will lead to an additional uncertainty of ± 0.01 and the estimated heat transport becomes 0.45 PW ± 0.17 PW.

July 2004

This line was conducted approximately along 37°S and is the southernmost section to date. During the month of July according to previous observations (i.e., Garzoli and Garraffo, 1989; Goni and Wainer, 2001), the Malvinas Current should be at its northernmost extension. The SST satellite image (Figure 9) shows the presence of the cold shelf water as far north as almost 31°S . As in the November 2002 section, it is confined to the shallow waters of the continental shelf (water depths < 200 m) and hence is likely a mixture of river outflow and cold/fresh southern shelf water. The westernmost station was collected near the 200 m isobath and therefore the section was completely sampled according to specification (e.g. the 0.01 PW typical correction for missing transport near the western boundary is unnecessary).

Due to malfunctioning equipment, the easternmost XBT stations were lost and the first good XBT was collected at 13.83°E . Hence, there is a need to account for the flow typically found between 13.83 and 17.5°E that was not sampled. The sea surface height map of the region (Figure 10, lower right panel, Goni personal communication) indicates the presence of an Agulhas ring centered at approximately $33^{\circ}30'\text{S}14^{\circ}30'\text{E}$, just east of where the first good XBT was deployed.

The missing flow was estimated in two different ways:

1. The values of dynamic height obtained with the altimeter data (Figure 8, lower right panel) estimate the missing transport as about 3 Sv. This missing volume transport leads to an increase in the heat transport of 0.15 PW.
2. The WOA01 data completes the section in the region of missing data. In this case the increase in the heat transport is 0.2 PW.

Without any correction for the missing flow at the boundaries, the heat transport estimate for the section is 0.53 PW. The average of the two corrections increases the heat transport by $+0.17 \pm 0.03$ PW. Adding this average correction to the uncorrected heat transport, the estimated net heat transport becomes 0.70 ± 0.19 PW

Similar calculations were made for reference level $\sigma_2=37.09 \text{ kg m}^{-3}$. The results of applying the methodology described above for the nine cruises are presented in Table III and Figure 11.

The section conducted during July 2002 was done along 30°S and is the only one at this location (see Table II). This location is similar to the one occupied during WOCE (A10). Comfortingly, but no doubt fortuitously, the value of the meridional heat transport obtained is very similar (0.49 ± 0.17 PW) to the one obtained for A10 (0.41 PW) using reference level $\sigma_2=37.09 \text{ kg m}^{-3}$. Results of applying this methodology to all the sections are give in Table III and Figure 11.

V. Conclusions

In summary, ten high-density XBT sections were used to infer the meridional heat transport in the South Atlantic. The values obtained for the heat transport (Table III and Figure 11) ranged from 0.4 to 1.0 PW with a mean value of 0.73 ± 0.17 PW when using $\sigma_0=27.4 \text{ kg m}^{-3}$ as the reference level and 0.67 ± 0.17 PW for $\sigma_2=37.09 \text{ kg m}^{-3}$. The analysis of Figure 11 does not show any clear annual cycle, in spite of large seasonal variations in the location and strength of the Brazil and Malvinas Currents and the seasonal nature of the wind fields. There is a very slight suggestion of a long-term trend in the heat transport values, with an average of 0.67 ± 0.06 (0.57 ± 0.05) PW for

the first five sections and 0.81 ± 0.07 (0.78 ± 0.07) PW for the last 5 sections (for the shallow and deep reference levels respectively). Given the large seasonal and internannual variability, the huge influence of the variable wind field, and the different latitudes of the sections, many more observations would be needed to assess the seasonal cycle much less climate trends in from these observations.

The methodology used to obtain the heat transport was examined in detail using several “test” cases as benchmarks. We showed that the method could essentially reproduce the values obtained using more sophisticated data and analysis with the WOCE hydrographic line A10. The analysis of the product of a numerical model confirmed that baroclinic estimates of the transports should be adjusted by the contribution of a strong barotropic component of the flow along the western boundary. It was also shown that, if the results from the analysis of A10 can be considered representative, by completing the vertical section bellow 850 m (the deepest values of data collected with XBT) with climatological fields introduces a change of +0.2 PW to the heat transport. When comparing to other estimates, it is possible that we have introduced a positive bias in our estimates due to the methodology of using a smoothed deep-water climatology and therefore our estimates may be high. We have, however, used an annual mean climatology and hence all the variability in heat transport is entirely due to the changing thermal structure of the upper water column, plus wind and boundary current changes. Even though the data collected by Argo profiling floats helped to improve the T/S relations in the region, still better subsurface climatology for the lower layers is needed in order to improve the results. The high-density lines AX18 are to be continued at the

rate of 4 per year. After a sufficient number of realizations, it is assumed that these heat transport estimates will become more robust.

Acknowledgements

This work would not have been possible without the support of Ms Qi Yao, who quality controlled the XBT data and performed all the calculations used in this paper. Lt. Cmdr Ariel Troisi and Fabian Vettere, collected the data along the AX18 transect. Robert Roddy, managed the logistics and operations that assured these cruises were completed. Dr. Carlisle Thacker, provided the T/S relations for the region. Dr. Gustavo Goni created all the satellite images. We are indebted to all of them for their collaboration and support of the program. This work would not have been possible except for the hospitality of the Maersk Company, the many captains and crews of the merchant vessels Justice Container, Maersk Hong Kong, Ever Genius, and especially the Ever Garden. This work is funded by the Office of Climate Observations and the National Oceanic and Atmospheric Administration.

References

Bang ND, A., WRH. 1974. Direct current measurements of a shelf-edge frontal jet in the southern Benguela system. *J. of Mar. Res.*, vol. 32, no. 3, pp. 405-417.

Chelton, D. B., M. G. Schlax, D. L. Witter, J. G. Richman, 1990. GEOSAT altimeter observations of the surface circulation of the Southern Ocean, *J. Geophys. Res. (C Oceans)*. Vol 95, no. C10, pp. 17877-903.

Cox, M. D. 1975. A baroclinic numerical model of the world ocean: Preliminary results. *In Numerical Models of the Ocean Circulation*, pp. 107-120.

[de las Heras, M. M.](#) and R. Schlitzer 1999. On the importance of intermediate water flows for the global ocean overturning. *J. Geophys. Res. (C Oceans)*. Vol. 104, no. C7, pp. 15515-15536.

de Ruijter W.P.M., E.J. D. Campos, S.A Cunningham, J. Donners, A.L. Gordon, J.R.E. Lutjeharms, R.P. Matano, D. Nof and A.R. Piola, 2004. The role of the South Atlantic and inter-ocean exchanges on the thermohaline circulation, 1st International Clivar Science Conference, Baltimore, MD.

[Donners, J.](#) and S. S. Drijfhout, 2004. [The Lagrangian View of South Atlantic Interocean Exchange in a Global Ocean Model Compared with Inverse Model Results](#). *J. Phys. Oceanogr.*, Vol. 34, no. 5, pp. 1019-1035.

Duncombe Rae, C., S. L. Garzoli, and A. Gordon, 1996. The eddy field of the southeast Atlantic Ocean: A statistical census from the Benguela Sources and Transport project. *J. Geophys. Res. - Oceans*, 101, (C5), 11,949-11,964.

Flood R.D. and A. N. Shore, 1988. Mud waves in the Argentine basin and their relationship to regional bottom circulation patterns. *Deep Sea Research*, 35, 943-971.

[Fu, L. L.](#) 1981. [The General Circulation and Meridional Heat Transport of the Subtropical South Atlantic Determined by Inverse Methods](#). *J. Phys. Oceanogr.*, vol. 11, no. 9, pp. 1171-1193.

Ganachaud, A.S. and C. Wunsch. 2003. Large-scale ocean heat and freshwater transports during the World Ocean Circulation Experiment. *J. Climate*, vol. 16, pp. 696-705.

[Garzoli, S. L.](#) and A. L. [Gordon](#). 1996. [Origins and variability of the Benguela Current](#). *J. Geophys. Res. (C OCEANS)*, vol. 101, no. 1, pp. 897-906.

[Garzoli, S. L.](#) 1993. [Geostrophic velocity and transport variability in the Brazil-Malvinas Confluence](#), *Deep-Sea Research (Part I, Oceanographic Research Papers)*, vol. 40, no. 7, pp. 1379-1403.

[Garzoli, S. L.](#), Z. [Garraffo](#), G. [Podesta](#), and O. [Brown](#). 1992. [Analysis of a general circulation model product. 1. Frontal systems in the Brazil/Malvinas and Kuroshio/Oyashio regions.](#) *J. Geophys. Res. (C OCEANS)*, vol. 97, no. C12, pp. 20117-20138.

Garzoli, S. L., P.L. Richardson, C.M. Duncombe Rae, D.M. Fratantoni, G.J. Goni and A.J. Roubicek, 1999. Three Agulhas Rings Observed During the Benguela Current Experiment” (*J. Geophys. Res.*, Vol 104,No C9, 20971-20985.

[Garzoli, SL](#); A. [Bianchi](#). 1987. Time-space variability of the local dynamics of the Malvinas-Brazil confluence as revealed by inverted echo sounders. *J. Geophys. Res. (C OCEANS)*, vol. 92, no. C2, pp. 1914-1922.

[Garzoli, SL](#); Z. Garaffo. 1989. Transports, frontal motions and eddies at the Brazil-Malvinas currents confluence. *Deep-Sea Res. (A OCEANOGR. RES. PAP.)*, vol. 36, no. 5A, pp. 681-703.

[Goni, G. J.](#), S. L. [Garzoli, S. L.](#) [Roubicek, A. J.](#) [Olson, D. B.](#) [Brown](#). Sept 1997. Agulhas ring dynamics from TOPEX/POSEIDON satellite altimeter data. *J. of Mar. Res.* Vol. 55, no. 5, pp. 861-883.

Goni, G. J. and I Wainer. Dec 2001. Investigation of the Brazil Current front variability from altimeter data. *J. of Mar. Res.* Vol. 106, no. C12, pp. 31,117-31,128.

[Gordon, A. L.](#) and C. L. [Greengrove](#). 1986. [Geostrophic circulation of the Brazil-Falkland confluence.](#) *Deep-Sea Res.*, vol. 33, no. 5A, pp. 573-585.

[Gordon, A. L.](#), R. F. [Weiss](#), W. M. [Smethie Jr.](#) and [Warner, M. J.](#) 1992. [Thermocline and intermediate water communication between the South Atlantic and Indian Oceans.](#) *J. Geophys. Res.*, vol. 97, no. C5, pp. 7223-7240.

[Gordon, A.L.](#) and C. L. [Greengrove](#). 1986. [Geostrophic circulation of the Brazil-Falkland confluence.](#) *DEEP-SEA RES.*, vol. 33, no. 5A, pp. 573-585.

Hanawa, K., P. Rual, R. Bailey, A. Sya and M. Szabados. 1995. A new depth-time equatin for Sippican or TSK T-7, T-6 and T-4 expendable bathythermographs (XBT), *DEEP-SEA RES.*, V42, no. 8, 1423-1451.

Hellerman, S. and M. Rosenstein. 1983. Normal monthly wind stress over the world ocean with error estimates. *Journal of Physical Oceanography* 13: 1093-1104.

[Lutjeharms, J. R. E.](#), R. C. A. [van Ballegooyen](#). 1988. [Anomalous upstream retroflection in the Agulhas Current.](#) *Science* (Washington), vol. 240, no. 4860, pp. 1770-1772.

Mazio, C. A. , Walter C. Dragani, Fernando J. Caviglia, and Jorge L. Pousab, 2004. Tidal Hydrodynamics in Golfo Nuevo, Argentina, and the Adjacent Continental Shelf. *Journal of Coastal Research*: Vol. 20, No. 4, pp. 1000–1011.

McDonagh, E. L., B.A. King. 2005. Oceanic Fluxes in the South Atlantic, Southampton Oceanography Centre, Empress Dock, Southampton, U.K., pp.109-122.

[Macdonald, A. M.](#), M. O. [Baringer](#) and [A. Ganachaud](#). 2001. [Heat transport and climate](#). *Encyclopedia of Ocean Sciences* - Vol. 2 (D-H). pp. 1195-1206.

[Matano, R. P.](#) and S. G. H. [Philander](#). 1993. Heat and mass balances of the South Atlantic Ocean calculated from a numerical model. *J. Geophys. Res. (C OCEANS)*, vol. 98, no. C1, pp. 977-984.

Nelson, G., 1989. Poleward motion in the Benguela area. In: Neshyba SJ, Mooers CNK, Smith RL, Barber RT (eds) Poleward Flows along Eastern Ocean Boundaries. Springer, New York. *Coastal and Estuarine Studies*, vol. 34, pp. 110-130.

Nelson, G. 1991. An equatorward jet wash of Cape Town. Abstract IAPSO Proceedings XX Assembly Vienna, pp. 189.

[Olson, D. B.](#), G. P. [Podesta](#), R. H. [Evans](#), and O. B. [Brown](#). 1988. Temporal variations in the separation of Brazil and Malvinas Currents. OCEANOGR. RES. PAP. vol. 35, no. 12, pp. 1971-1990.

[Olson, D. L.](#), S. [Ibarra](#), and C. E. [Grubbs](#). 1988. Metallurgical aspects of underwater welding. ARO-23474.23-MS, 1988, 3 pp.

Palma, E.D., R.P. Matano, A.R. Piola y L.E. Sitz, 2004. The impact of wind climatologies on the modeled barotropic circulation of the Southwestern Atlantic Continental Shelf, *Geophys. Res. Lett.*, **31**, L24303, doi:10.1029/2004GL021068.

Parker, G; Paterlini, MC; Violante, RA; Boschi, EE , 1997. The sea floor, INIDEP. Instituto Nacional de Investigacion y Desarrollo Pesquero, Mar del Plata (Argentina).

Peterson, RG , 1988. On the transport of the Antarctic Circumpolar Current through Drake Passage and its relation to wind. *Journal of Geophysical Research. C. Oceans*. Vol. 93, no. C11, pp. 13993-4004.

[Peterson, R.G.](#) 1992. The boundary currents in the western Argentine Basin. DEEP-SEA RES. (A OCEANOGR. RES. PAP.), vol. 39, no. 3-4A, pp. 623-644.

[Piola, A. R.](#), [Gordon, A](#) 1989. [Intermediate waters in the southwest South Atlantic](#). Deep-Sea Research [DEEP-SEA RES.], vol. 36, no. 1A, pp. 1-16.

Reid, J. L. 1989. On the total geostrophic circulation of the South Atlantic Ocean: flow patterns, tracers and transport. *Progress in Oceanography*, 23, 149-244.

Richardson, P.L., and S.L. Garzoli. 2003. "Characteristics of intermediate water flow in the Benguela Current as measured with RAFOS floats". *Deep-Sea Research, Part II*, 50 (1): 87-118.

Rintoul, S. R. 1991. South Atlantic interbasin exchange. *J. Geophys. Res.*, 96, pp. 2675-2692.

Saunders P. M. and B. A. King. 1995. Oceanic fluxes on the WOCE A11 section, *Journal of Physical Oceanography*, vol. 25, no. 9, pp. 1942-1958.

[Saunders, P. M.](#) and S. R. [Thompson](#). 1993. Transport, heat, and freshwater fluxes within a diagnostic numerical model (FRAM). *J. PHYS. OCEANOGR.* vol. 23, no. 3, pp. 452-464.

[Semtner, A. J.](#) and R. M. [Chervin](#). 1992. [Scientific development of a massively parallel ocean climate model. Progress report, 1991-1992.](#) REP. U.S. DEP. ENERGY, 4 pp.

Shannon, L.V., and G. Nelson. 1996. The Benguela: Large Scale Features and Process and System Variability, pp. 163-210. Springer-Verlag, Berlin, in: *The South Atlantic: past and present circulation* (Wefer, Berger, Siedler, and Webb ed.)

Shannon, LV., Lutjeharms JRE, Agenbag, JJ. 1989. Episodic input of Subantarctic water into the Benguela region. *S Afr J Sci* 85 (5): 317-322.

Siedler, G., T.J. Mueller, R. Onken, M. Arhan, H. Mercier, B. A. King and P.M. Saunders. 1996. The zonal WOCE sections in the South Atlantic, pp 83-104. Springer-Verlag, Berlin, in: *The South Atlantic: past and present circulation* (Wefer, Berger, Siedler and Webb ed.).

Smith, W. H. F., and D. T., 1997. Sandwell, Global seafloor topography from satellite altimetry and ship depth soundings, *Science*, v. 277, p. 1957-1962, 26 Sept.

Stephens, J. I., T. P. Antonov, T. P. Boyer, M. E. Conkright, R. A. Locarnini, T. D. O'Brien and H. E. Garcia, *World Ocean Atlas 2001*, ., 2002. Vol 1: Temperatures, S. Levitus, ed., NOAA Atlas, NESDIS 49, U. S. Government Printing Office, Wash., D.C., 176 pp.

Stramma, L. and England, M. 1999. On the water masses and mean circulation of the South Atlantic Ocean. *J. Geophys. Res.*, vol.104, no. C9, pp. 20,863-20,883.

[Stramma, L.](#) and R. G. [Peterson](#). 1990. [The South Atlantic Current.](#), *Journal of Physical Oceanography* [*J. PHYS. OCEANOGR.*], vol. 20, no. 6, pp. 846-859.

[Talley, L. D.](#) Mar 2003. Shallow, Intermediate, and Deep Overturning Components of the Global Heat Budget. *J. Phys. Oceanogr.*, Vol. 33, no. 3, pp. 530-560.

Thacker, W. C., S.-K. Lee, and G. R. Halliwell. 2004. Assimilating 20 years of Atlantic XBT data into HYCOM: A first look. *Ocean Modelling*, 7(1-2):183-210.

Tokmakian, R.T. and Challenor, P.G. 1999 On the joint estimation of model and satellite sea surface height anomalies. *Ocean Modelling*, 1, 39-52.

Vivier, F; C. Provost, and M. P. Meredith, 2001. Remote and Local Forcing in the Brazil-Malvinas Region. *Journal of Physical Oceanography* [J. Phys. Oceanogr.]. Vol. 31, no. 4, pp. 892-913.

[Webb, D. J. et al., 1991. An eddy-resolving model of the Southern Ocean. *EOS-Trans. Am. Geophys. Union.*, vol. 72, no. 15.](#)

Figure Captions

Figure 1: A schematic representation of the large-scale circulation of North Atlantic Deep Water (NADW) (yellow), Antarctic Intermediate Water (AAIW) (red), and South Atlantic Central Water (SACW) (blue). Adapted from the results from Stramma and England (1999).

Figure 2: Location of the 10 transects conducted along the XBT high-density line AX18.

Figure 3: Temperature section from the data collected along the WOCE A10 line (heavy white lines represent density surfaces discussed in text).

Figure 4: Time series of the total heat transport (top panel) at 35°S obtained from the POCM velocity and temperature fields. The lower panel is the climatological annual cycle of the heat transport (1986-1998) computed from the full time series.

Figure 5: Ekman heat flux in PW as a function of time and latitude calculated from the NCEP climatological monthly winds. Values presented as heat flux, H_y , where $H_y = M_y * c_p * (T_{Ekman} - T_{section})$. The Ekman layer temperature, T_{Ekman} , is computed from WOA01 assuming a ΔT of 0.1°C from the surface. $T_{section}$ is the spatial average of the WOA01 annual mean section.

Figure 6: Monthly NCEP winds (top) superimposed to the cruise track (solid red line) and sea surface temperature during the time of the March 2002 cruise.

Figure 7: Average SST for the duration of the cruise (top panel) conducted during November 2002. The solid line indicates the ship track. Lower panels are details of SST at the boundaries.

Figure 8: Sea surface height derived from altimeter anomalies courtesy of G. Goni for November 2002. The top panel shows the fields along the cruise track (solid line) and the lower panels details at the boundaries.

Figure 9: Same as Figure 5 for July 2004.

Figure 10: Same as Figure 6 for July 2004.

Figure 11: Heat transport from data collected during the different cruises. Top: plotted as an annual cycle, bottom: as time series. indicate values obtained using σ_0 as the reference level indicate values obtained using σ_2 as reference level. Vertical lines indicate the error bars.

Table Captions

Table I: Heat transport estimates for WOCE A10 section using several assumptions and simplifications to the data (see text).

Table II: Detailed specification of average positions of each XBT section. “XBT dpth” indicates the maximum depth to which good temperature data was collected from the XBT and “ocean dpth” the depth of the ocean at that same location.

Table III: Heat transport estimates for each of the XBT transects. “Date” is the date when the cruise was started, “Ekman” is the Ekman heat flux, Boundaries indicate when a correction made at the boundaries, “geostrophic” is the geostrophic component of the heat transport and “Total HT” is the final value obtained for the heat transport. All units are PW ($1\text{PW} = 10^{15}$ Watts).

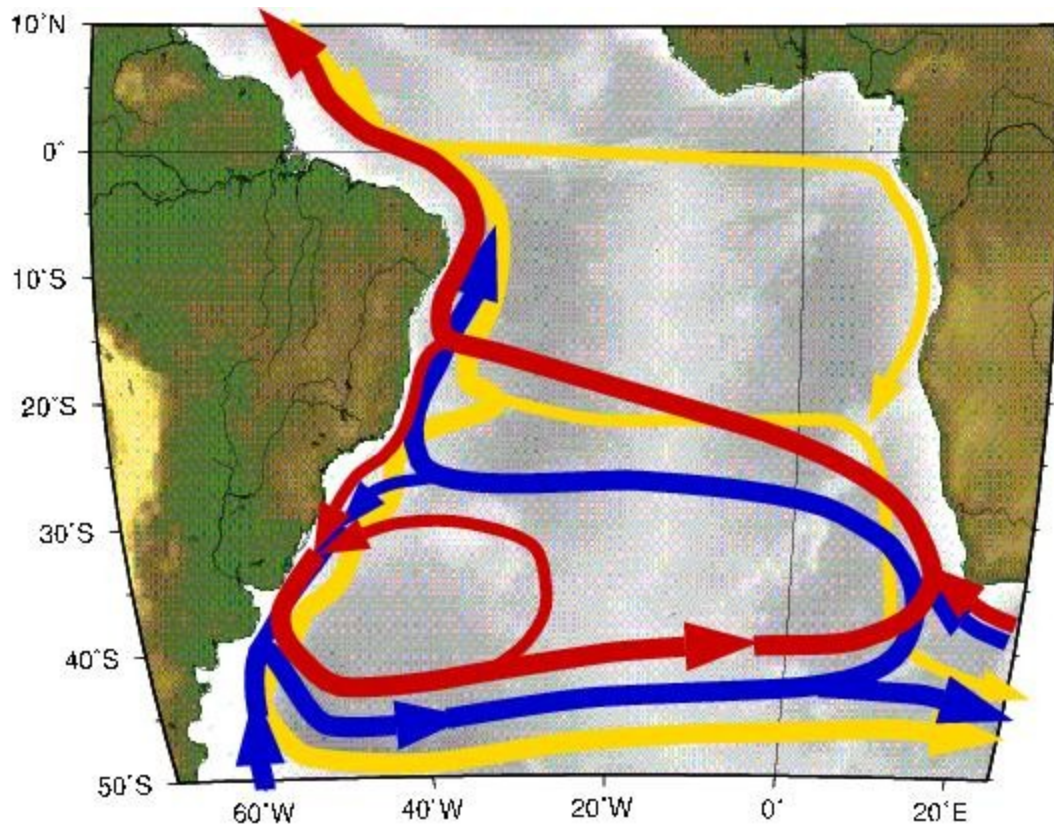


Figure 1

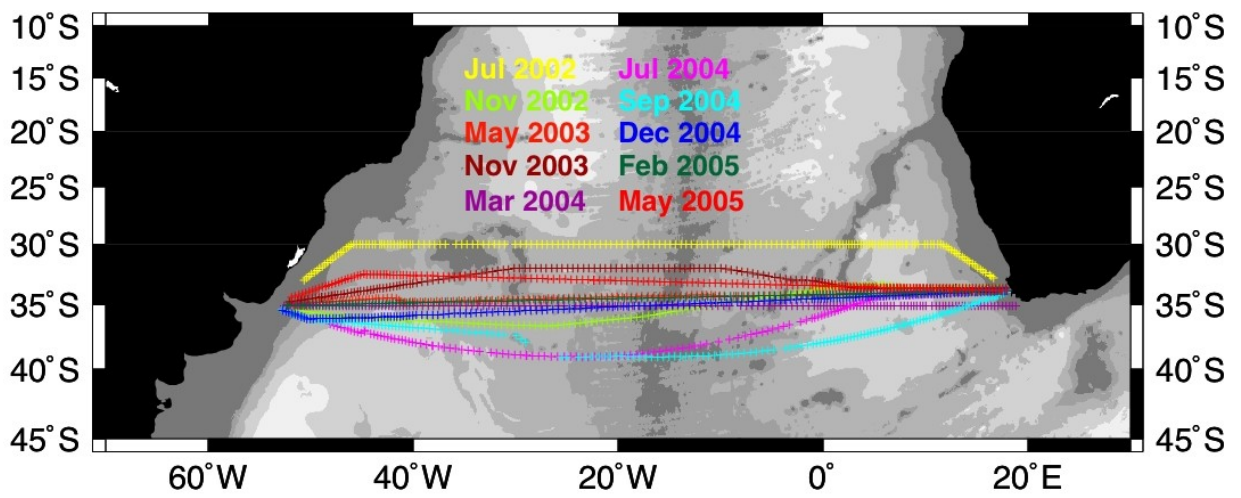


Figure 2

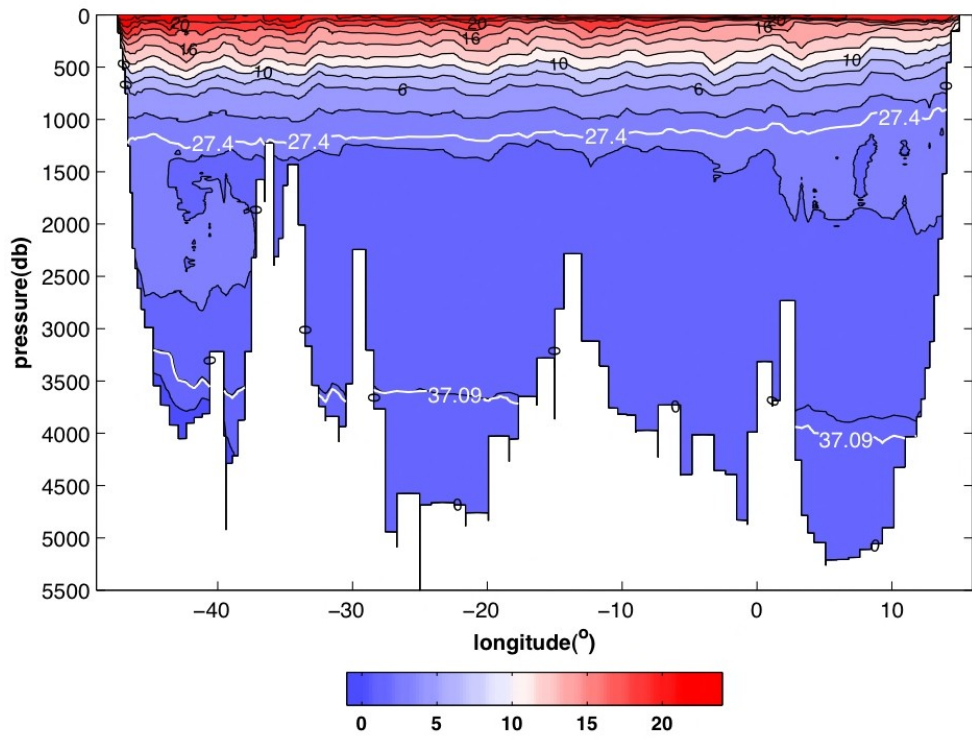
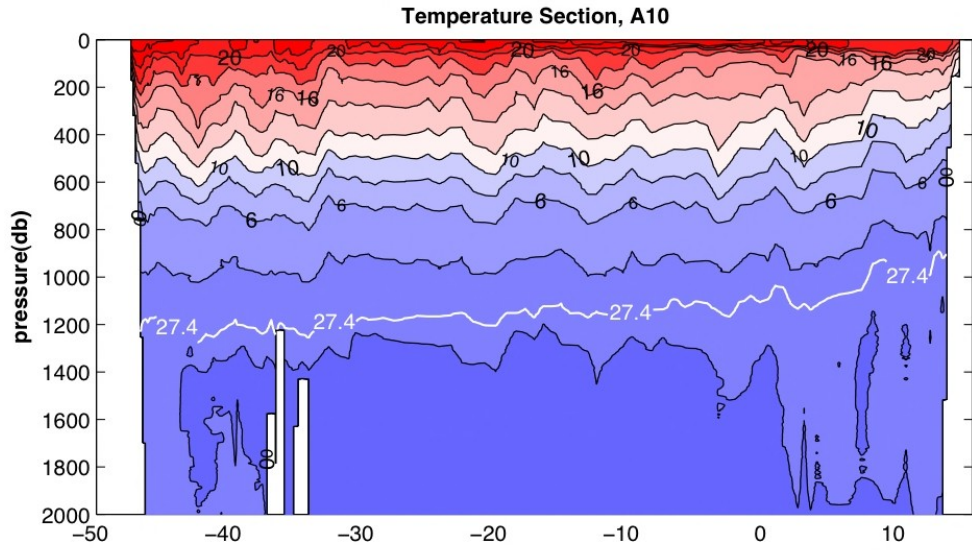
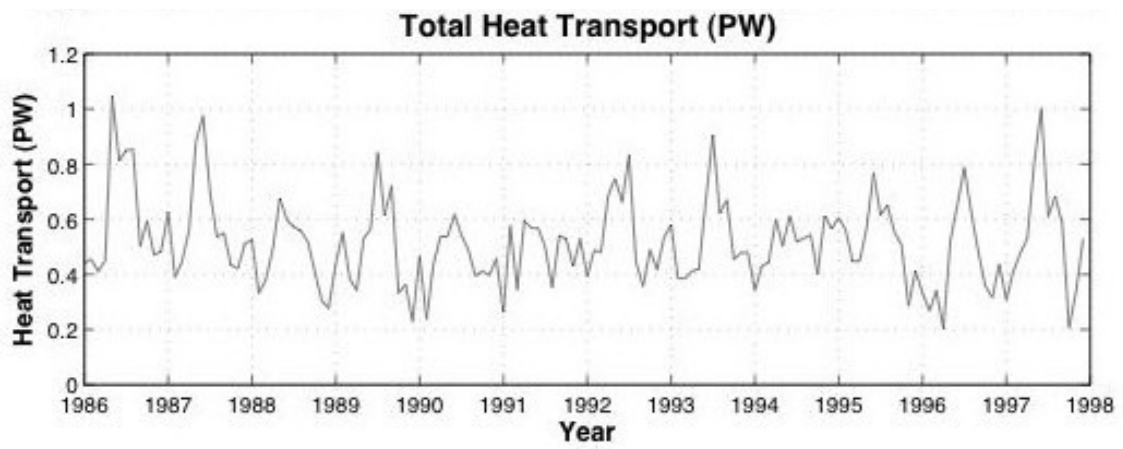


Figure 3



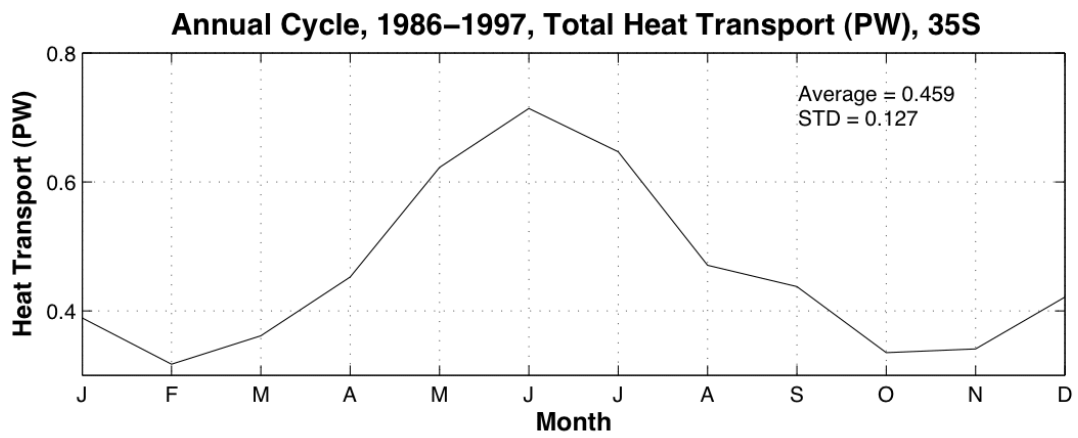
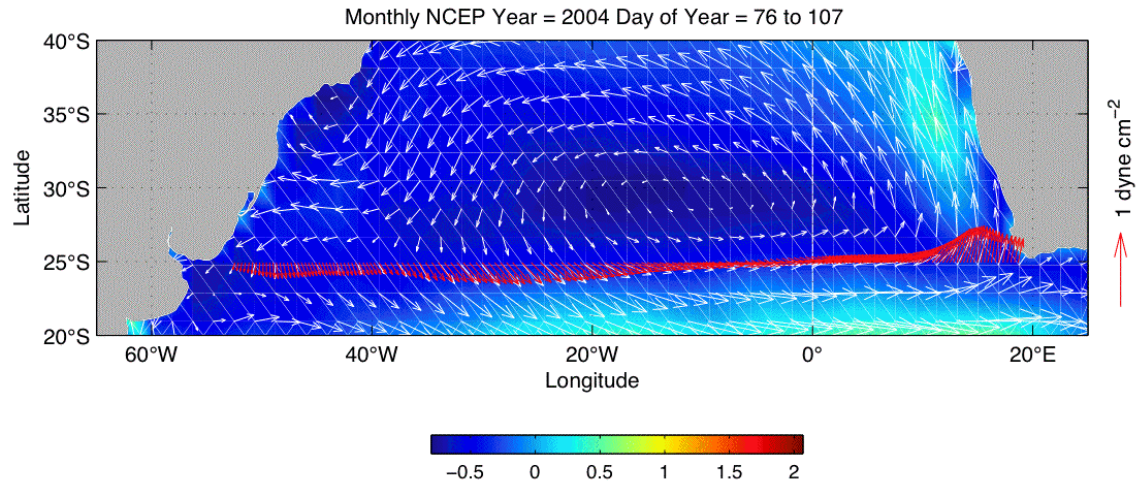


Figure 4

Figure 5



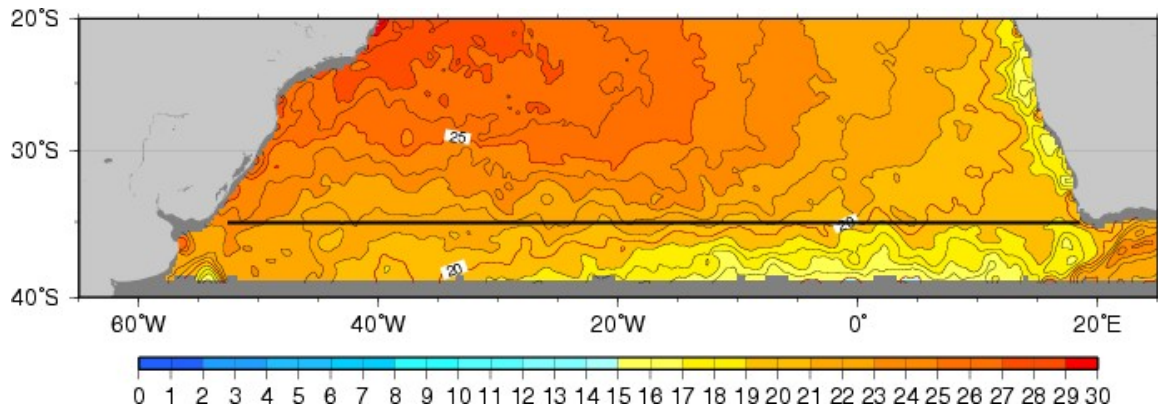


Figure 6

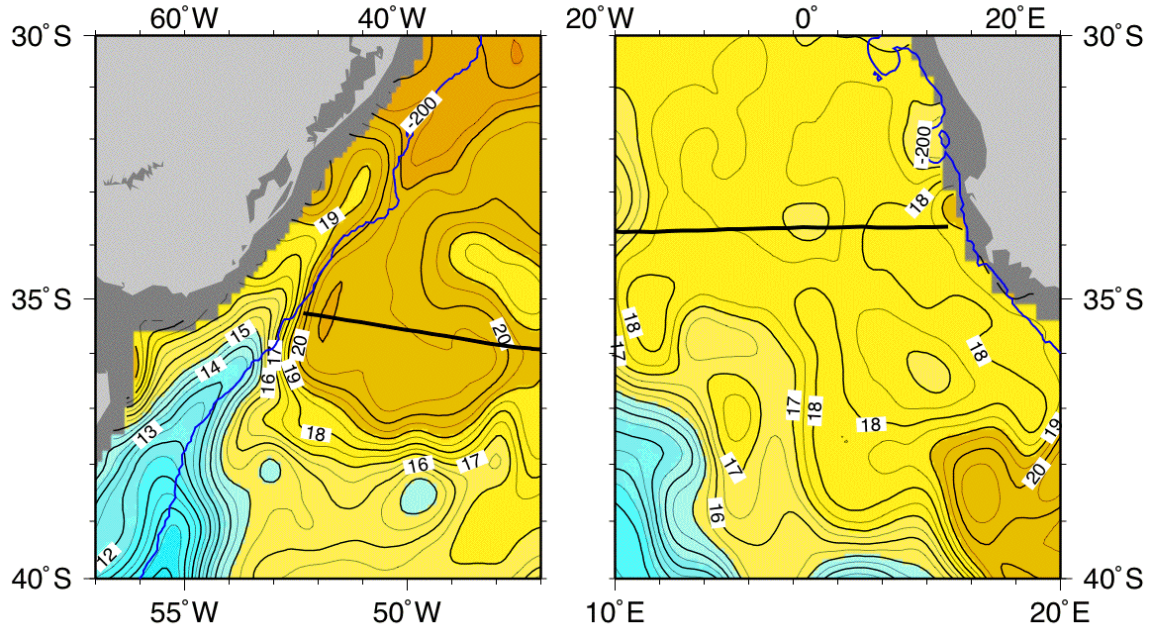
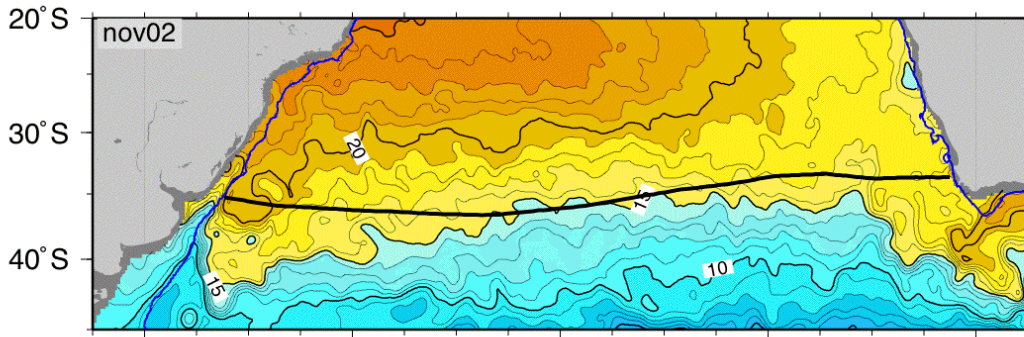


Figure 7

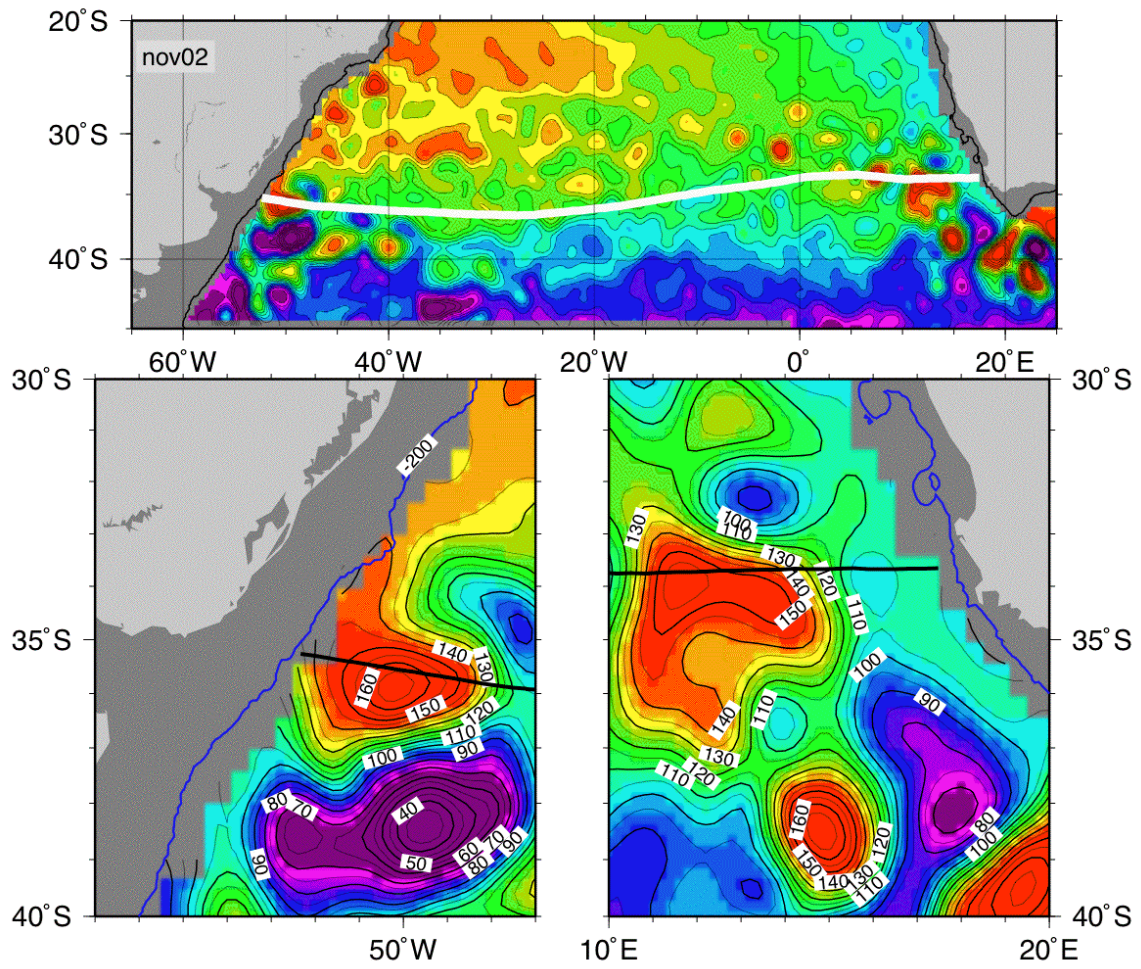


Figure 8

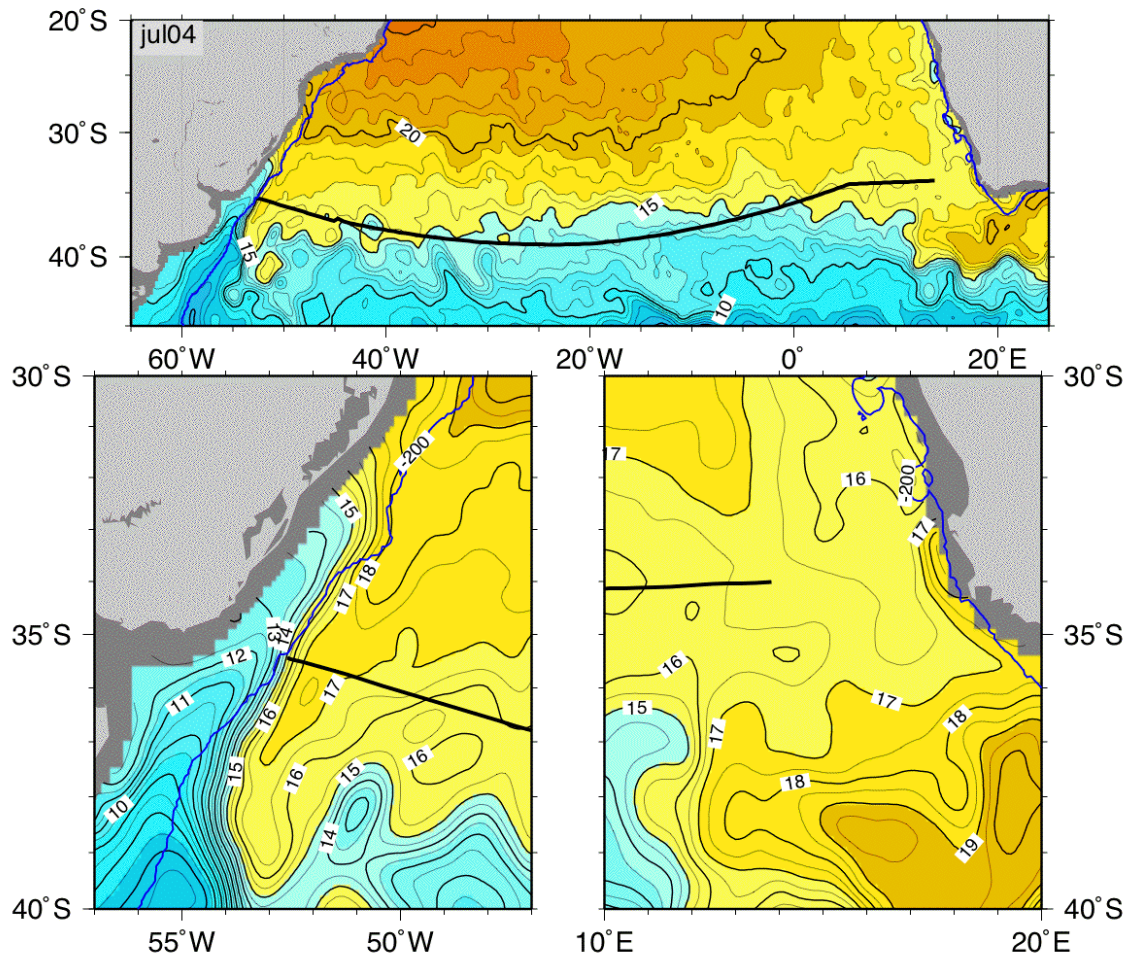


Figure 9

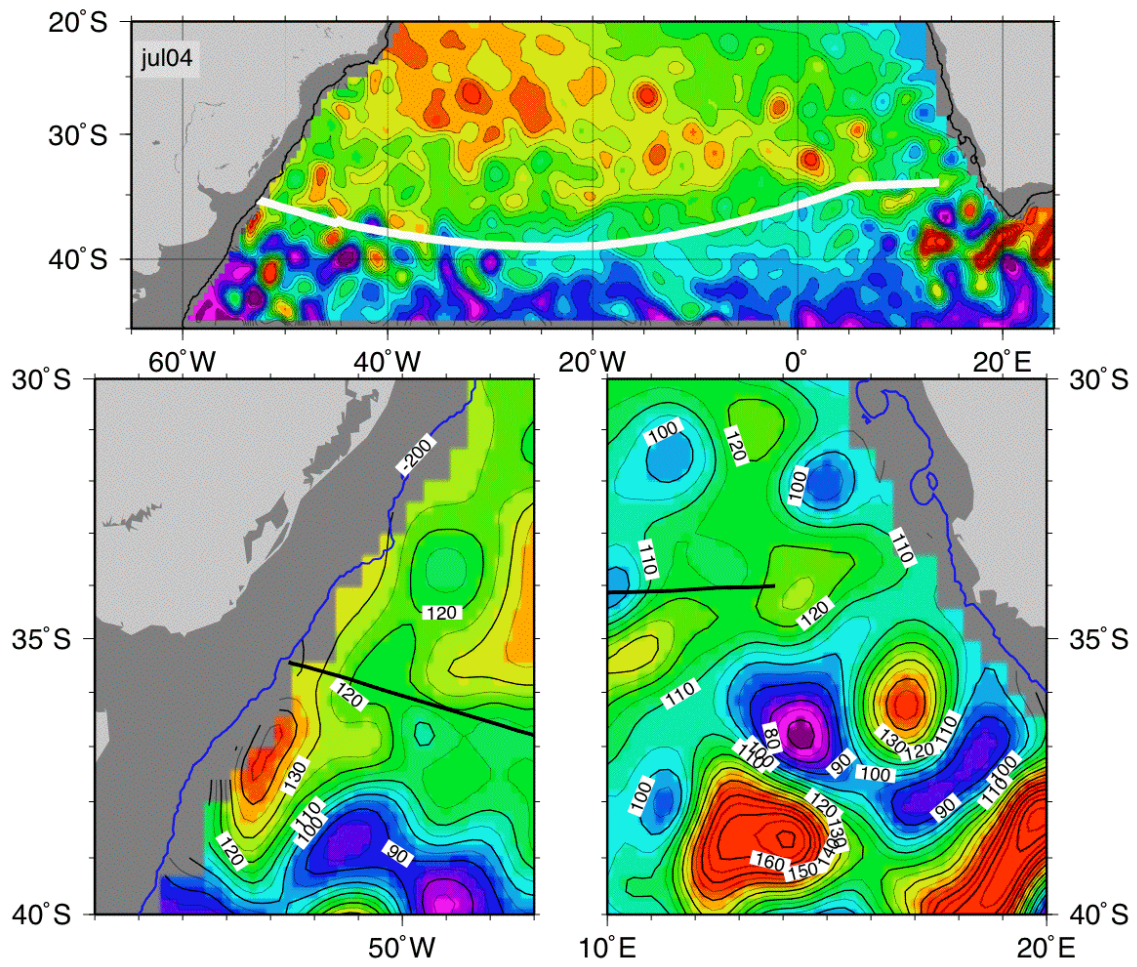
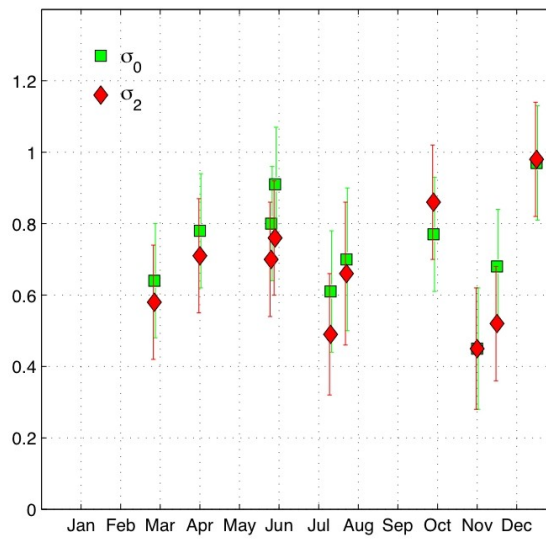


Figure 10



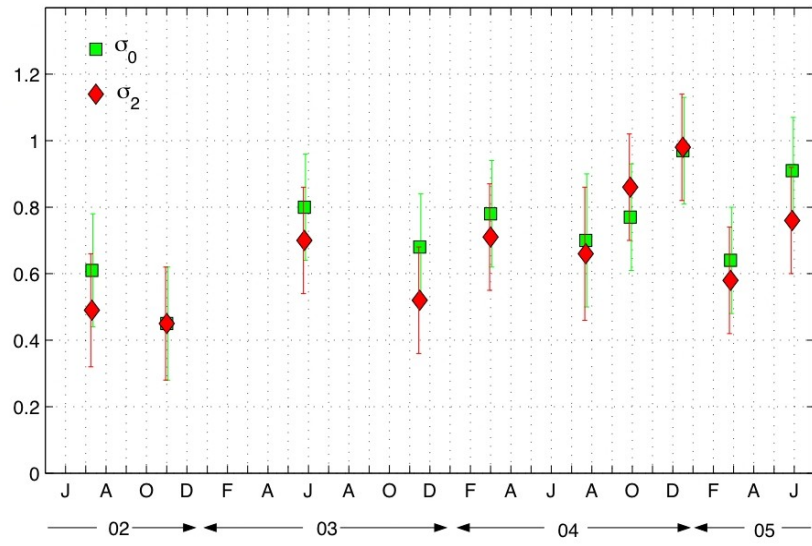


Figure 11

Heat Transport

Reference level:	$\sigma_1=37.07 \text{ kg m}^{-3}$	$\sigma_1=27.4 \text{ kg m}^{-3}$
1 Ganachau and Wunsch (2003)	0.40 PW	N/A
2 Direct estimate	0.41 PW	0.60 PW
3 T(z) from A10, S(T,P) above 850 m	0.45 PW	0.64 PW
4 WOA01 bellow 850 m	0.66 PW	0.75 PW
5 Bottom from Smith and Sandwell	0.69 PW	0.78 PW

Table I:

Table II

month	year	Western lon	Wester n lat	XBT dpth	ocean dpth	Eastern lon	Easter n lat	XBT dpth	ocean dpth	Mean Lat
		°W	°S	m	m	°E	°S	m	m	°S
July	2002	-50.64	-32.99	84	177	16.66	-32.81	860	862	-30.0
November	2002	-52.33	-35.26	814	832	17.48	-33.66	791	793	-35.0
May	2003	-52.39	-34.99	153	155	17.89	-33.87	209	212	-34.3
November	2003	-52.1	-34.75	195	198	17.84	-33.67	197	198	-33.1
March	2004	-52.6	-35.07	128	129	18.82	-35.07	219	272	-35.1
July	2004	-52.59	-35.44	200	200	13.83	-34.00	820	4427	-36.8
September	2004	-52.8	-35.41	118	129	17.94	-33.96	202	204	-37.0
December	2004	-52.74	-35.43	210	210	18.00	-33.87	173	175	-35.0
February	2005	-52.3	-35.04	160	190	17.86	-33.86	213	220	-34.4
May	2005	-51.85	-34.4	153	155	17.8	-33.85	254	256	-33.2

Table III

Date	Ekman	Boundaries	Geostrophic	Total HT	Geostrophic	HT
			$\sigma_0=27.4 \text{ kg m}^{-3}$	$\sigma_0=27.4 \text{ kg m}^{-3}$	$\sigma_2=37.09 \text{ kg m}^{-3}$	$\sigma_2=37.09 \text{ kg m}^{-3}$
Jul-02	0.09	-0.01	0.53	0.61 ± 0.17	0.41	0.49 ± 0.17
Nov-02	0.08	-0.02	0.39	0.45 ± 0.17	0.39	0.45 ± 0.17
May-03	0.23	-0.01	0.58	0.80 ± 0.16	0.48	0.70 ± 0.16
Nov-03	0.03	n/a	0.65	0.68±0.16	0.49	0.52±0.16
Mar-04	0.02	n/a	0.76	0.78 ± 0.16	0.69	0.71 ± 0.16
Jul-04	0.26	0.17	0.27	0.70 ± 0.20	0.23	0.66 ± 0.20
Sep-04	0.17	n/a	0.6	0.77±0.16	0.69	0.86±0.16
Dec-04	0.12	n/a	0.85	0.97±0.16	0.86	0.98±0.16
Feb-05	0.00	n/a	0.64	0.64±0.16	0.58	0.58±0.16
May-05	0.21	n/a	0.7	0.91±0.16	0.55	0.76±0.16

All units are PW (1 PW = 10¹⁵ Watts)